

On the Effect of Imperfect Reference Images in SAR Change Detection Based on Bayes' Theorem

Lucas Pedroso Ramos, Rômulo Fernandes da Costa, Diego da Silva de Medeiros, Paulo Ricardo Branco da Silva, Dimas Irion Alves, and Renato Machado

Abstract—This paper presents a study regarding the impact of using imperfect reference images containing targets and artifacts in the performance of change detection methods. The presented analysis uses a change detection method based on Bayes' Theorem recently proposed. The experimental evaluation is carried out using wavelength-resolution SAR images obtained using the CARABAS II SAR system. The experimental setup considers two types of reference images, i.e., imperfect and ground scene prediction (GSP) generated images. The imperfect images are those available in the dataset. The GSP-generated images are obtained by the GSP method and tend not to contain targets and artifacts. Results indicate that the use of reference images obtained by the GSP method provides a false alarm reduction in the evaluated scenarios when compared with the CDA implementation with imperfect reference images. For instance, a FAR reduction from 0.667 to 0.229 is observed in an evaluated setup.

Keywords—Change detection method, ground scene prediction, Synthetic Aperture Radar (SAR), wavelength-resolution SAR images.

I. INTRODUCTION

Synthetic aperture radar (SAR) is an important tool for imaging the Earth's surface. By choosing an appropriate operation frequency, it is possible to obtain an accurate image of the surface without the need for solar light and under detrimental weather conditions such as fog, rain, and snow [1]. These characteristics make SAR imaging attractive for both civilian [2] and military applications [3]. Of particular interest are SAR systems operating at lower frequencies, with wavelengths comparable with the dimensions of a resolution cell. These wavelength-resolution systems can be used for natural disaster monitoring and detecting targets concealed in foliage [4]. Due to the longer wavelength, speckle is reduced in the processed SAR image, and smaller objects such as small tree branches, forest canopies, or ground vegetation of the illuminated area are effectively eliminated from the image, as these objects create a negligible backscatter compared to larger objects in the resolution cell [5], [6].

Change detection in wavelength-resolution SAR is an important processing strategy for target detection. A change

detection algorithm (CDA) detects differences between images of the same area obtained at different times and classifies them on a binary basis as either changed or unchanged [7]. In [8], discrete wavelet transform is applied to the differential image obtained through mean-ratio and log-ratio operations to detect changes. In [9], a CDA technique based on a neighborhood-based ratio operator is presented. More recently, deep learning techniques have been used in change detection. For example, in [10], images that first undergo morphological operations are processed by a deep belief network to create a change map. In [11], stacked contractive autoencoders are employed to suppress the influence of speckle noise in the change map. Convolutional neural networks are also used in change detection, such as in [12] and [13]. However, significant drawbacks of deep-learning-based approaches include a high requirement of data for training and the relatively high complexity of these methods.

A simple CDA derived from an approximation of Bayes' theorem was presented in [14]. This CDA uses a single reference image to detect changes and estimate the probability of change for each pixel in the surveillance image. This method uses the joint probability distribution and the histograms estimated from reference and surveillance images. The estimate can then be compared to a fixed threshold. The method is simple and interpretable, but it improves over traditional methods in terms of detection and false alarm rates. Also, it can be used with limited data, unlike data-intensive procedures such as machine learning techniques.

CDA performance depends on how well the reference image corresponds to the actual ground truth. It was verified in [15] that image stacks could yield better detection results since the additional information is used to reduce the influence of imperfections in the reference image caused by elongated structures such as fences and power lines. It is possible to perform GSP with the image stack, creating an accurate reference image. For instance, in [16], median pixel values of a stack of wavelength-resolution images create an accurate representation of the ground scene from a probability distribution perspective.

The main objective of this paper is to discuss the effect of using imperfect reference images in CDAs, where imperfection is defined as the presence of targets and artifacts in the image. To this end, an experimental setup is used based on real data obtained by the CARABAS II system. The performance of a CDA based on Bayes' Theorem [14] is evaluated in two scenarios: one using imperfect images and another using reference images obtained from a GSP procedure [16]. The GSP procedure tends to mitigate targets and artifacts. The

Lucas Pedroso Ramos, Rômulo Fernandes da Costa, Diego da Silva de Medeiros, Paulo Ricardo Branco da Silva, Dimas Irion Alves, and Renato Machado are Aeronautics Institute of Technology (ITA), São José dos Campos-SP, Brazil. Email: (lucaspr, rfcosta, rmachado, dimasirion)@ita.br. Diego da Silva de Medeiros is also with Federal Institute of Santa Catarina, São José-SC, Brazil, e-mail: diegomedeiros@ifsc.edu.br; Paulo Ricardo Branco da Silva is also with Centro de Pesquisa e Desenvolvimento em Telecomunicações (CPqD), Campinas-SP, Brazil, e-mail: pauloricardo.branco@gmail.com.

results indicate that the use of GSP-generated reference images reduces the false alarm rate in the evaluated scenarios compared to the original implementation with imperfect reference images.

The rest of this work is organized as follows. Section II briefly describes the experimental data. Section III describes the CDA based on Bayes' Theorem. Section IV presents the GSP method under analysis. Results are presented in Section V, and Section VI contains final remarks.

II. CARABAS-II SAR DATA SET

Of the wavelength-resolution SAR systems available [15], one that has been proven efficient for change detection applications is the CARABAS-II, which produces SAR images at the very high frequency (VHF) band (20-90 MHz) [4]–[17]. This study considers 24 SAR images acquired by the CARABAS-II system during a measurement campaign carried out in northern Sweden in 2002. These images were documented in [7] and are publicly available by the U.S. Air Force Research Lab (AFRL) on the sensor data management system (SDMS) website [18]. Each image of the data set is formed by 3000×2000 pixels and covers an area of 6 km^2 . The area is characterized by the presence of forested regions, rivers, transmission lines, and fences. Also, 25 military vehicles were inserted in order to represent the targets of the scene [7].

The images can be grouped into four different missions, representing four different target deployments. In this study, we adopt the same nomenclature of [7], where the missions are referred to as 2, 3, 4, and 5. Each mission is represented by six platform passes performed with different flight headings. Let 0° be defined as the north heading and let the heading angle increase in the clockwise direction. Two passes were made with a flight heading of 225° , two with a flight heading of 135° , and two with a flight heading of 230° . Figure 1 shows the images for each mission.

III. CDA BASED ON BAYES' THEOREM

A. Overview

This section briefly describes the change detection method based on Bayes' Theorem presented in [14]. Bayes' theorem describes how the conditional probability of an event A , given prior knowledge of a second event B , correlates to the probabilities $P(A)$ and $P(B)$, with the variation

$$P(A|B) = \frac{P(B|A)P(A)}{P(B)}, \quad (1)$$

where $P(B|A)$ is the probability of event B given prior knowledge of event A .

Change detection in SAR can be formulated in terms of Bayes' Theorem by considering the relations between data in two complex images: the reference and surveillance images. The reference image is used to measure the clutter present in the scene, while the surveillance image has as its focus target detection. Following Bayes' theorem, the probability of the pixel under test z_U in the surveillance image being detected

as a change in relation to the same pixel z_R in reference image is

$$P(s_T|z_U, z_R) = \frac{P(z_U|s_T, z_R)P(s_T|z_R)}{P(z_U|z_R)}, \quad (2)$$

where s_T is the event of an actual change in the pixel under test. The opposite event where there are no changes in the pixel under test is denoted as s_C . The probability $P(s_T|z_R)$ describes the probability of the evaluated pixel containing a target given z_R , and since the presence of a target is independent of z_R , it can be written as

$$P(s_T|z_R) = P(s_T) = \frac{MK}{N}, \quad (3)$$

where M is the number of pixels occupied per change, i.e., target footprint, K is the number of detected changes, and N is the number of pixels in the image.

The probability of a pixel amplitude z_U occurring given z_R can be described as $P(z_U|z_R)$. Additionally, this probability $P(z_U|z_R)$ can be represented by the probability of the two mutually exclusive events s_T and s_C , and thus can be formulated as

$$P(z_U|z_R) = P(z_U|s_T, z_R)P(s_T) + P(z_U|s_C, z_R)[1 - P(s_T)]. \quad (4)$$

Isolating $P(z_U|s_T, z_R)$, we have

$$P(z_U|s_T, z_R) = \frac{P(z_U|z_R) - P(z_U|s_C, z_R)[1 - P(s_T)]}{P(s_T)}. \quad (5)$$

We then replace (5) in (2) to obtain

$$P(s_T|z_U, z_R) = 1 - \frac{P(z_U|s_C, z_R)[1 - P(s_T)]}{P(z_U|z_R)}. \quad (6)$$

Considering that $N \gg MK$ and following the algebraic manipulations in [14], $P(s_T|z_U, z_R)$ can be approximated by

$$P(s_T|z_U, z_R) \approx 1 - \frac{P(z_U, z_R|s_C)}{P(z_U, z_R)}. \quad (7)$$

The probability $P(z_U, z_R|s_C)$ can be obtained from a probability distribution function modeling the background of the SAR images, while $P(z_U, z_R)$ is obtained directly from a histogram of the SAR image. Assuming that an appropriate pdf is chosen to represent $P(z_U, z_R|s_C)$, then the presence of a change will result in $P(z_U, z_R)$ increasing in relation to $P(z_U, z_R|s_C)$ and as consequence $P(s_T|z_U, z_R)$ increases and approaches 1. If $P(s_T|z_U, z_R)$ exceeds a predefined threshold λ , a detection is declared.

B. Clutter-Plus-Noise Model

Traditionally, used distributions for modeling SAR images are the bivariate Rayleigh, bivariate Gamma, and K-distributions [19], [17]. The bivariate Rayleigh is used in this work for modeling $P(z_U, z_R|s_C)$, because of its simplicity

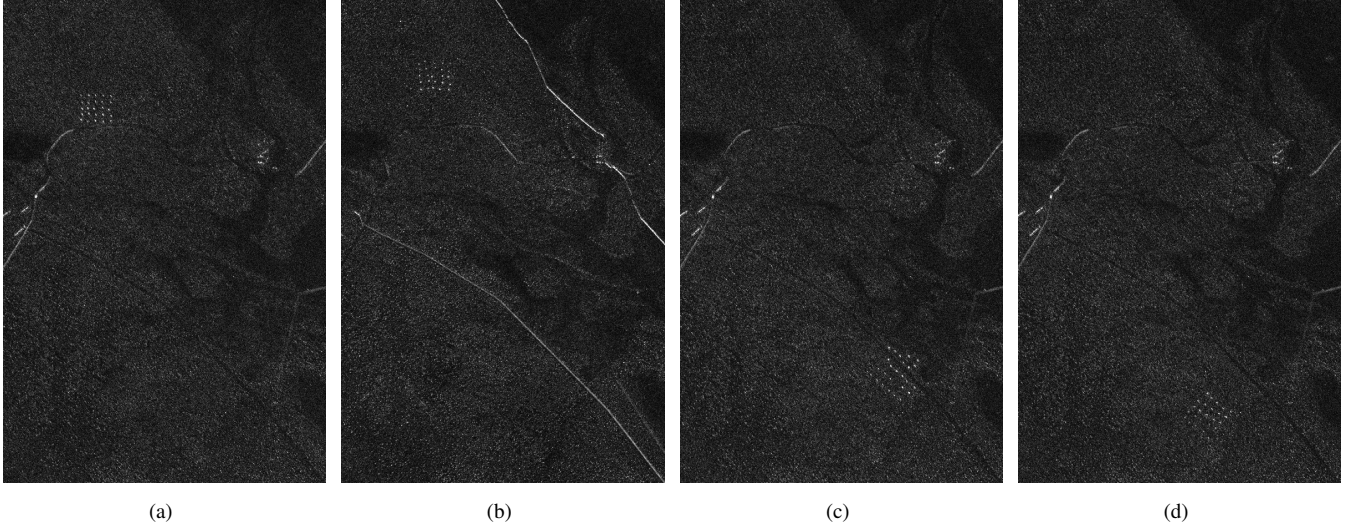


Fig. 1. Magnitude of CARABAS-II SAR images in different missions: (a) Mission 2, Pass 1 (225°); (b) Mission 3, Pass 2 (135°); (c) Mission 4, Pass 5 (230°); and (d) Mission 5, Pass 6 (230°).

and effectiveness in change detection applications [19], [20]. The Rayleigh bivariate probability distribution function is

$$f_{z_U, z_R}(z_U, \Omega_U; z_R, \Omega_R | \rho) = \frac{4z_R z_U}{\Omega_R \Omega_U (1 - \rho)} \exp \left[-\frac{1}{1 - \rho} \left(\frac{z_R^2}{\Omega_R} + \frac{z_U^2}{\Omega_U} \right) \right] \times I_0 \left(\frac{2\sqrt{\rho}}{1 - \rho} \frac{z_R z_U}{\sqrt{\Omega_R \Omega_U}} \right), \quad (8)$$

where $\Omega_R = \bar{z}_R^2$ and $\Omega_U = \bar{z}_U^2$, with \bar{z}_U and \bar{z}_R representing mean values of z_U^2 and z_R^2 , respectively. $I_0(\cdot)$ is the zero-order modified Bessel function, and ρ the correlation coefficient of z_R^2 and z_U^2 , is given by

$$\rho = \frac{\text{cov}(z_U^2, z_R^2)}{\sqrt{\text{var}(z_U^2) \text{var}(z_R^2)}}, \quad (9)$$

where cov and var denote covariance and variance, respectively. The parameters of this distribution can be estimated directly from the whole image data in the surveillance and reference images via a maximum-likelihood estimator.

C. Change Detection Method

From the knowledge of the probability distribution functions (pdf) of $P(z_U, z_R)$ and $P(z_U, z_R | s_C)$, it is possible to calculate $P(s_T | z_U, z_R)$ for every pixel in the surveillance image. To reduce runtime processing, the computation in (7) is only applied to positive changes in z_U that satisfy $z_U > z_R + \Delta z$. Δz is a small increment in magnitude from the reference image, chosen according to prior knowledge of the image data statistics. Based on the previous consideration, only targets appearing in z_u are computed as changes. The probability $P(s_T | z_U, z_R)$ is automatically clamped to zero if the condition is not satisfied. Moreover, $P(z_U, z_R | s_C)$ is clamped to 0 in case (7) becomes negative due to a mismatch in the choice of the distribution model in $P(z_U, z_R | s_C)$ and the data histogram.

A binary map is generated for the surveillance image, comparing it to a threshold λ , with every pixel assigned the

value of 1 for $P(s_T | z_U, z_R) \geq \lambda$ and 0 otherwise. The CDA as described is illustrated in Figure 2. Erosion and dilation are applied to this binary mask to remove small false alarms and merge fragmented detections. It was originally implemented in [14], referred to as non-iterative Bayes' theorem CDA.

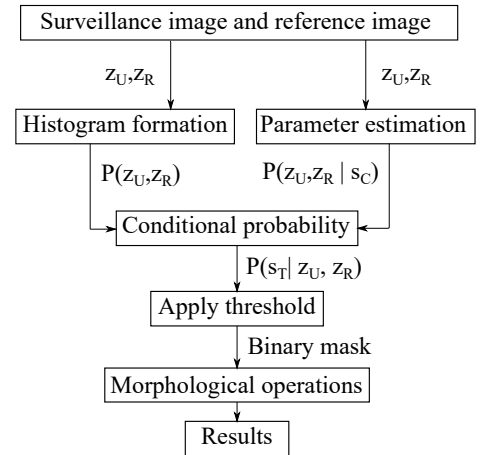


Fig. 2. Block diagram of the evaluated CDA based on the Bayes' theorem.

IV. GROUND SCENE PREDICTION

The target detection performance of a CDA is highly dependent on the fidelity of the reference image to the ground scene. Often in change detection applications, a single pair of images taken from an image data set is used as surveillance and reference images, with the reference image frequently having interfering targets and other artifacts [14], [15], [17], [20]. One way to avoid this problem is through GSP approaches over an image stack, where a better reference image can be obtained.

Recently, [16] proposes a GSP based on auto-regressive models for the following metrics, median, mean, trimmed mean, and intensity mean. The reference image from the GSP was tested in a CDA, and it was verified that the median

provided a more accurate representation of the reference images in terms of the average, standard deviation, skewness, kurtosis, as well as goodness-of-fitness measures like the mean absolute percentage error and the median absolute error [16]. Three different stacks with eight images can be formed from the CARABAS II data. These stacks are composed of images with similar flight headings [5], [16], creating stability over time. We define stability as the relative invariability of the image statistics. Following [16], we refer to 225° , 135° , and 230° stacks as numbers 1, 2, and 3, respectively. Once the stack is formed with the targets in different positions (i.e., two images of each mission within the stack), applying these statistical methods will mitigate the pixels-amplitude related to the presence of targets from the image stack. Consequently, the GSP can be obtained, as shown in Figure 3.

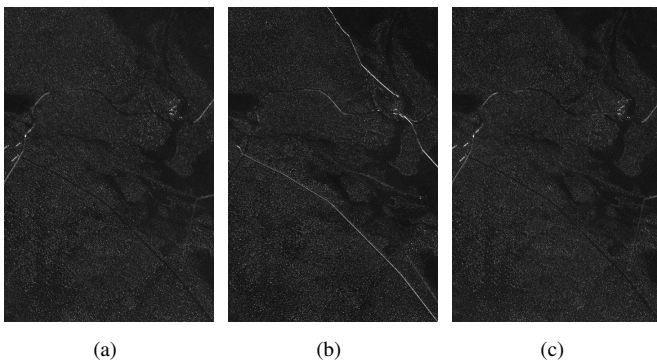


Fig. 3. GSP image obtained for three stacks using the median (adapted from [16]): (a) Stack 1 (225°); (b) Stack 2 (135°); and (c) Stack 3 (230°).

V. EXPERIMENTAL RESULTS

To assess the impact of using target-free reference images, we present an experimental evaluation based on the CDA presented in [14], assuming the reference images are generated via the median method in [16]. Herein, the proposed method is named the median-based GSP method over the Bayes' theorem CDA. The experimental evaluation considers all the 24 images from the data set presented in Section II. The methods' performance is assessed in terms of the probability of detection (P_d), i.e., the ratio of the number of detected targets to the known number of targets, and the false alarm rate (FAR) - here defined as the number of false alarms per square kilometer. For the analysis, every object detected by the method was considered a change, even those produced by target fragmentation and image formation issues.

The first comparison in Figure 4 is between the receiver operating characteristic (ROC) curve with the reference as a GSP-generated image and the ROC curve produced with the standard reference images in [14]. For the sake of simplicity, we adopted the same image pairs as in [14] and [7]. The detection threshold λ is varied across a wide range of values to measure the probability of detection P_d as a function of FAR. The values of Δz were the same used in [14] and [17], i.e., $[0.2, 0.3, 0.4]$. The curves with the same colors and markers were obtained using the same values for Δz , with the solid line representing the CDA using GSP, and the dashed line the original implementation presented in [14].

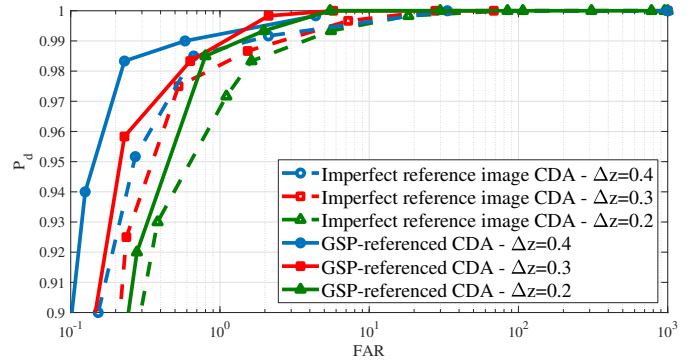


Fig. 4. The probability of detection P_d as a function of FAR for the original implementation of the Bayes' Theorem-based CDA (dashed lines) and for the implementation using median-based GSP (solid lines)

It can be noticed that, as a result of the more accurate reference image provided by the GSP, i.e., no targets and fewer artifacts, there was a significant improvement in reducing the FAR. For the case of $\Delta z = 0.4$, P_d is approximately 97.4% for a FAR of about 0.2 using the median-based GSP implementation against a P_d approximately equal to 92.4% for the imperfect reference image implementation. For a comparatively higher FAR of about 1, P_d is approximately 99.2% using the median-based GSP implementation against a $P_d \approx 98.7\%$ for the imperfect reference image implementation.

To further investigate the effects of reference images, we present the results for a specific test setup in Table I, as evaluated in [14]. For fair comparisons and readability, we should have practically the same P_d in the two scenarios. As can be observed, for the approximate P_d of 0.985, the FAR reduced from 0.667 to 0.229. This reduction is mainly due to the removal of targets and image artifacts from the reference images. As discussed in [14], this adverse effects require more sophisticated false alarm reduction techniques than the ones considered in [14]. Indeed, using reference images in CDA from GSP methods is a possible way to reduce the occurrence of false alarms related to these issues.

VI. CONCLUSION

This paper presents a preliminary study regarding the impact of using reference images containing targets and artifacts (imperfect images) in the performance of change detection methods for wavelength-resolution SAR images. This initial analysis uses a recently proposed change detection method based on Bayes' theorem. It is important to emphasize that most of the CDA proposed for wavelength-resolution SAR images use reference images contaminated by targets. For comparison purposes, we used imperfect or GSP-generated images as reference images as input of the studied CDA. Experiments were performed for the CARABAS-II data set. A performance improvement was observed in all evaluated scenarios when GSP-generated images were used. Also, we observed that the GSP strategy could be extended to other change detection algorithms and SAR data sets.

TABLE I

 PERFORMANCE COMPARISON BETWEEN CDA WITH IMPERFECT REFERENCE IMAGE (IRI-CDA) [14] AND CDA WITH GSP-REFERENCED (GSP-CDA) FOR $\lambda = 0.3$ AND $\Delta z = 0.4$.

Experiment Number	Surveillance Image		Detected Targets (IRI-CDA)	Probability of Detection (IRI-CDA)	False Alarms (IRI-CDA)	FAR (IRI-CDA)	Detected Targets (GSP-CDA)	Probability of Detection (GSP-CDA)	False Alarms (GSP-CDA)	FAR (GSP-CDA)
	mission	pass								
1	2	1	25	1	0	0	25	1	0	0
2	3	1	25	1	6	1	25	1	3	0.5
3	4	1	25	1	0	0	25	1	0	0
4	5	1	25	1	4	0.67	25	1	2	0.33
5	2	2	25	1	0	0	25	1	0	0
6	3	2	25	1	0	0	25	1	0	0
7	4	2	25	1	1	0.17	25	1	1	0.17
8	5	2	25	1	0	0	25	1	0	0
9	2	3	25	1	2	0.33	25	1	1	0.17
10	3	3	24	0.96	0	0	24	0.96	0	0
11	4	3	25	1	2	0.33	25	1	2	0.33
12	5	3	25	1	2	0.33	25	1	0	0
13	2	4	25	1	0	0	25	1	0	0
14	3	4	25	1	0	0	25	1	0	0
15	4	4	25	1	1	0.17	25	1	1	0.17
16	5	4	23	0.92	1	0.17	23	0.92	0	0
17	2	5	25	1	2	0.33	25	1	0	0
18	3	5	19	0.76	54	9	18	0.72	23	3.83
19	4	5	25	1	0	0	25	1	0	0
20	5	5	25	1	21	3.5	25	1	0	0
21	2	6	25	1	0	0	25	1	0	0
22	3	6	25	1	0	0	25	1	0	0
23	4	6	25	1	0	0	25	1	0	0
24	5	6	25	1	0	0	25	1	0	0
Total			591	0.985	96	0.667	590	0.983	33	0.229

ACKNOWLEDGMENTS

This work was supported in part by the Brazilian Agencies National Council for Scientific and Technological Development (CNPq), Saab AB, the Coordination for the Improvement of Higher Education Personnel (CAPES) – Finance Code 001 (Pró-Defesa IV), and the BIOS - Brazilian Institute of Data Science, grant 2020/09838-0, São Paulo Research Foundation (FAPESP).

REFERENCES

- [1] Y. S. Tsai, A. Dietz, N. Oppelt, and C. Kuenzer, "Remote sensing of snow cover using spaceborne SAR: A review," *Remote Sensing*, vol. 11, no. 12, p. 1456, 2019.
- [2] C. Liu, Z. Chen, S. Yun, J. Chen, T. Hasi, and H. Pan, "Research advances of SAR remote sensing for agriculture applications: A review," *Journal of integrative agriculture*, vol. 18, no. 3, pp. 506–525, 2019.
- [3] G. G. Schaber, "SAR studies in the Yuma Desert, Arizona: Sand penetration, geology, and the detection of military ordnance debris," *Remote sensing of environment*, vol. 67, no. 3, pp. 320–347, 1999.
- [4] H. Hellsten, L. M. Ulander, A. Gustavsson, and B. Larsson, "Development of VHF CARABAS II SAR," in *Radar Sensor Technology*, vol. 2747. International Society for Optics and Photonics, 1996, pp. 48–60.
- [5] R. Machado, V. T. Vu, M. I. Pettersson, P. Dammert, and H. Hellsten, "The stability of UWB low-frequency SAR images," *IEEE Geoscience and Remote Sensing Letters*, vol. 13, no. 8, pp. 1114–1118, 2016.
- [6] Z. Xu, "Wavelength-resolution sar speckle model," *IEEE Geoscience and Remote Sensing Letters*, vol. 19, pp. 1–5, 2022.
- [7] M. Lundberg, L. M. Ulander, W. E. Pierson, and A. Gustavsson, "A challenge problem for detection of targets in foliage," in *Algorithms for Synthetic Aperture Radar Imagery XIII*, vol. 6237. International Society for Optics and Photonics, 2006, p. 62370K.
- [8] J. Ma, M. Gong, and Z. Zhou, "Wavelet fusion on ratio images for change detection in SAR images," *IEEE Geoscience and Remote Sensing Letters*, vol. 9, no. 6, pp. 1122–1126, 2012.
- [9] M. Gong, Y. Cao, and Q. Wu, "A neighborhood-based ratio approach for change detection in SAR images," *IEEE Geoscience and Remote Sensing Letters*, vol. 9, no. 2, pp. 307–311, 2011.
- [10] F. Samadi, G. Akbarizadeh, and H. Kaabi, "Change detection in SAR images using deep belief network: A new training approach based on morphological images," *IET Image Processing*, vol. 13, no. 12, pp. 2255–2264, 2019.
- [11] N. Lv, C. Chen, T. Qiu, and A. K. Sangaiah, "Deep learning and superpixel feature extraction based on contractive autoencoder for change detection in SAR images," *IEEE Transactions on Industrial Informatics*, vol. 14, no. 12, pp. 5530–5538, 2018.
- [12] H. M. Keshk and X.-C. Yin, "Change detection in SAR images based on deep learning," *International Journal of Aeronautical and Space Sciences*, vol. 21, no. 2, pp. 549–559, 2020.
- [13] L. Li, C. Wang, H. Zhang, B. Zhang, and F. Wu, "Urban building change detection in SAR images using combined differential image and residual u-net network," *Remote Sensing*, vol. 11, no. 9, p. 1091, 2019.
- [14] D. I. Alves, B. G. Palm, H. Hellsten, V. T. Vu, M. I. Pettersson, R. Machado, B. F. Uchôa-Filho, and P. Dammert, "Wavelength-resolution SAR change detection using Bayes' theorem," *IEEE Journal of Selected Topics in Applied Earth Observations and Remote Sensing*, vol. 13, pp. 5560–5568, 2020.
- [15] V. T. Vu, "Wavelength-resolution SAR incoherent change detection based on image stack," *IEEE Geoscience and Remote Sensing Letters*, vol. 14, no. 7, pp. 1012–1016, 2017.
- [16] B. G. Palm, D. I. Alves, M. I. Pettersson, V. T. Vu, R. Machado, R. J. Cintra, F. M. Bayer, P. Dammert, and H. Hellsten, "Wavelength-resolution SAR ground scene prediction based on image stack," *Sensors*, vol. 20, no. 7, p. 2008, 2020.
- [17] V. T. Vu, N. R. Gomes, M. I. Pettersson, P. Dammert, and H. Hellsten, "Bivariate gamma distribution for wavelength-resolution SAR change detection," *IEEE Transactions on Geoscience and Remote Sensing*, vol. 57, no. 1, pp. 473–481, 2018.
- [18] U.S. Air Force. The Sensor Data Management System. Accessed May 3, 2022. [Online]. Available: <https://www.sdms.afri.af.mil>
- [19] N. R. Gomes, M. I. Pettersson, V. T. Vu, P. Dammert, and H. Hellsten, "Likelihood ratio test for incoherent wavelength-resolution SAR change detection," in *IEEE CIE International Conference on Radar (RADAR)*, 2016, pp. 1–4.
- [20] V. T. Vu, M. I. Pettersson, and N. R. Gomes, "Stability in SAR change detection results using bivariate Rayleigh distribution for statistical hypothesis test," in *IEEE International Geoscience and Remote Sensing Symposium (IGARSS)*, 2019, pp. 37–40.